

FLYORIEN: A BIO-INSPIRED MODEL FOR INCREMENTAL LEARNING OF OBJECT ORIENTATION

Anonymous authors

Paper under double-blind review

ABSTRACT

Visual orientation detection helps navigation, especially without a reliable magnetic compass or GPS. Inspired by the neural mechanisms of the insect brain, particularly the mushroom body (MB) and the central complex (CX), we propose FlyOrien—a bio-inspired model for object orientation detection. The model mimics the MB for random feature extraction, sparse coding and associative learning, while the CX provides multi-clue sensory integration, enabling interpolation for finer orientation representation. FlyOrien’s biologically plausible learning rule allows one-shot learning, reducing the need for large datasets and repeated training. We tested FlyOrien on a dataset containing images labeled with orientations, which introduce strong interferences because images of the same object have different labels. In this challenging context, FlyOrien achieves competitive performance compared to convolutional neural networks (CNNs), significantly reducing training time and computational resources. It also has the potential for real-world applications like robotics, where incremental learning is essential.

1 INTRODUCTION

In a natural environment, many clues can indicate directions, such as the direction of the sun, the skylight polarisation, upwind direction, and landmarks. Animals can use them for direction and navigation (Heinze, 2017). Most of these clues are perceived by vision. Even simple insects can use vision memory to remember the way home by finding a familiar direction that allows its route after walking along the route once, the underlying mechanism has been partly explained with the Mushroom body (Ardin et al., 2016), a learning center in insects (for a review, see Modi et al. (2020)). Their lightweight neural circuits are faster than typical artificial neural networks (ANN) in remembering orientations. Hence, we investigated these circuits for an architecture and learning rule to retrieve orientation memory for vision signals.

Our intention to retrieve orientation is related to object pose estimation but focuses on the relative directions between an observer and an object on the ground. A typical object pose estimation process either has a planar feature reference for a flat face of the object or has a 3-dimensional (3D) reference, such as a CAD model, for the shape of the object (Van de Ven et al., 2022). With the reference, the pose object in the image can be estimated. These types of models are applied in AprilTag (Olson, 2011), human face orientation detection, and industrial robot piece picking (Fan et al., 2022). In a natural environment, objects with a flat surface are not common, and animals also do not have a predefined 3D reference. For the purpose of navigation on the ground, the relative horizontal direction of an animal to an object is more important than the pose of the object. Hence, our model focused on the relative horizontal direction but not pose estimation.

Assuming an observer always faces an object, with a reference direction, which could be true north, there are three orientations: the angle the observer facing to o , the angle the object is facing to o' , and the relative angle between the two angles $o - o'$. If we knew two of them, the third can be computed. If o and $o - o'$ are known, it is an object-orienting problem. o' and $o - o'$ are known, it is an observer orienting problem. For simplification, in the object orienting problem, o is 0, and in the object orienting problem o' is 0. Hence, in our dataset, there is only one number as a label for each sample, and the two problems are not distinguished explicitly in our paper. By discretizing the range from 0° to 360° to multiple discrete values, the object orientation detection task can be set as a multi-class classification problem.

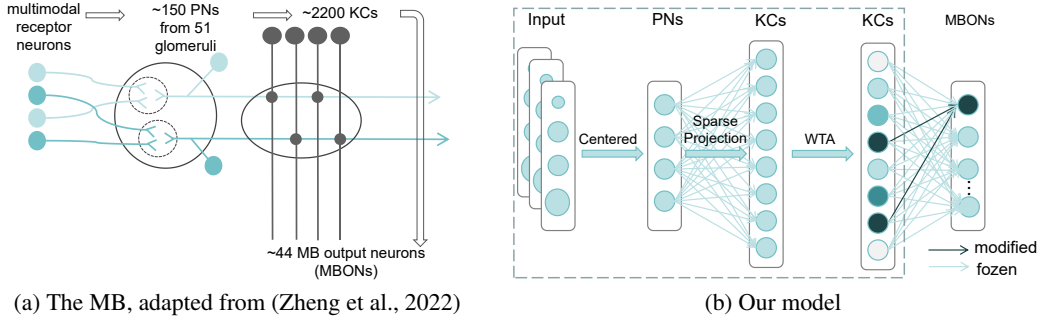


Figure 1: Schematics diagram of the MB and the simplified MB model in FlyOrien. (a) The MB of a larval fruit fly *Drosophila melanogaster*, illustrating connections from sensors to the MB output neurons. (b) The simplified MB model in FlyOrien. The dashed line frames the parts for random feature extraction. Only weights between this part and “MBONs” are adjust during learning.

There have been many models for finding objects’ orientation in the plane of the image but not horizontally on the ground, for example, PSC (Yu & Da, 2023), TIOE-Det (Ming et al., 2023) and ReDet (Han et al., 2021). These works are an extension of traditional object detection but use a rotated bounding box, and treat the rotation angle as orientation. Their application includes aerial images (Xia et al., 2018), scene text (Ma et al., 2018), and industrial inspection (Wu et al., 2022). These methods typically involve deep networks requiring prolonged training time and random shuffling of many data samples for training. For near-ground navigation using vision, a landmark object typically has a fixed orientation relative to its surroundings. As a result, the angle within the view plane is less important than the direction in which the object is facing the viewer.

An insect can remember the orientation of a landmark by looking at it once without buffering the image data (Jeffery et al., 2016). Hence, it is interesting to explore how insects can do it and use its underlying mechanism for orientation retrieval or detection. Insect’s neural circuit is capable of sparse coding without learning, and the resulting sparse representation reduces conflicts in learning (Pearce & Bouton, 2001). The mushroom body (MB) (Figure 1a) of *Drosophila* is a typical example. The neural system of *Drosophila* has been closely observed, 3D reconstructed, and analyzed for its connectome (Li et al., 2020b). With the information, we can have a more accurate interpretation of how it may work.

The MB receives multimodal sensory inputs that are preprocessed by upstream circuits and delivered by the projection neurons (PNs) (Hallem & Carlson, 2006; Stevens, 2016). Each Kenyon cell (KC) in the MB receives the signals from a special combination of several PNs (typically 3 to 5) (Olsen et al., 2010), and the group of KCs together encode the signals in a sparse coding manner. Only a small section of KCs, typically 5% to 15%, can fire at the same time, because a neuron called APL (anterior paired lateral neuron) receives from all KCs and inhibits them (Caron et al., 2013). The axons of the KCs pass through multiple compartments, each of which typically has one mushroom body output neuron (MBON) for output and one Dopaminergic neuron for reward and learning modulation. Because the number of KCs is much larger than PNs and the sparse activities of KCs (Aso et al., 2014), existing connections between KCs and MBONs are less likely to be impacted by later learning.

The MB has been model for olfactory associative learning or decision-making, during with odor signals are sent to the MB by antennal lobe projection neurons. Wessnitzer et al. (2007) proposed a model with Izhikevich neurons and an STDP learning rule for non-elemental associative learning. Smith et al. (2008) proposed an MB model with integrate-and-fire (IF) neurons and an activity-dependent pre-synaptic facilitation (APDF) learning rule for associative learning. More recently, Bennett et al. (2021) modeled the MB with dopamine neurons for signaling reinforcement prediction errors instead of reward to explain blocking experiments.

Biological experiments and computational neuroscience models suggest that the insect MB plays an important role in insect navigation (Webb & Wystrach, 2016), such as visual homing. The visual inputs to the mushroom body mainly from visual projection neurons (VPNs) nerved from the optic

lobe and intermediate local visual interneurons (LVINs)(Ganguly et al., 2024; Li et al., 2020a). When a desert ant leaves its nest foraging, its pheromones vaporize away in high temperatures. Hence, it has to rely on skylights and landmarks for navigation. Ardin et al. (2016) proposed an MB model, in which an ant sees the surrounding environment, and an MBON can indicate unfamiliarity of the heading direction according to vision inputs. According to this model, an ant can learn familiarity with scene orientation during the route leaving home, then go back by searching the most familiar coming direction. Based on it, Zhu et al. (2020) proposed a model with Leaky-Integrated-Fire (LIF) neurons and a modified STDP learning rule to learn on an event-based camera (also called dynamic vision sensor (DVS)) for visual homing. Although there are differences between the connections, the MB are assumed to use similar ways for coding, and previous experiments has shown it is functional (Ardin et al., 2016; Dasgupta et al., 2017; Wei et al., 2022; Zhu et al., 2020).

The architecture of the MB has inspired researchers in computer science to propose models for fundamental problems such as Locality Sensitive Hashing(LSH). Typical LSH algorithms reduce the dimension of the original data for hashing (Gionis et al., 1999), FlyLSH (Dasgupta et al., 2017) algorithm increases the dimension in the first step by mapping data samples with a random sparse binary projection matrix. It mimics the almost random connections from PNs to KCs (Caron et al., 2013; Baltruschat et al., 2021; Hayashi et al., 2022). The mapping result is binarized by setting the strongest dimensions to one and the others to zero, which is a form of the k-Winner-Take-All (k-WTA) process. The resulting binary vector is the hash code. The FlyLSH algorithm performs well in the nearest neighbor retrieval task of the images. The schematic plot of FlyLSH is presented in the dashed line zone of Figure 1b.

Another circuit that proved essential in navigation is the central complex (CX) (Honkanen et al., 2019). The neurons in the CX form a ring attractor, and encode the information of heading direction and homing direction in a group coding manner. It can merge multiple direction clues to find a direction more accurately than relying on a single clue (Heinze, 2017). The neurons representing different directions integrate heading directions with respect to movement speed, enabling the CX to calculate and remember both the direction and distance from the nest (Stone et al., 2017; Francoville et al., 2018). Neuron activities predicted by computational neuroscience models with a ring attractor match biological observations.

The function of the CX can be modeled and explained by the Continuous Attractor Neural Network(CANN), which forms a ring attractor and neurons encode information in a group coding manner(Wu et al., 2016). When there is external signal input, the network generates a Gaussian-shaped wave packet activity. The dynamics of CANN can function as a filter in time and space tendering the jitters of input signals. For head direction coding, the head direction neurons in the brain are interconnected through mutual feedback to form a one-dimensional CANN (Zhang, 1996). The collective activity of neurons in the network dynamically creates a Gaussian wave packet, with the peak position of the wave packet encoding the head direction. As the head rotates, the wave packet in the network can rotate accordingly due to sensory inputs and network dynamics, retaining information about head direction.

The connectome of *Drosophila* shows that 22 out of 34 MBON types connect to the fan-shaped body in the CX (Li et al., 2020a), which means the output of MBON contributes to the direction memorized by the insect. This combination allows the coordination of these two functions: the MB matches familiar vision inputs with long-term memory by synaptic plasticity, and the CX provides a more continuous decision for direction steering.

Inspired by the MB and the CX, we proposed a model called FlyOrien for incremental learning of the relative direction between an observer and an object given a side view of the object. We also propose biologically plausible learning rules that enable one-shot learning and incremental learning with FlyOrien, reducing training time and computational resource requirements. The model is different from CNNs in that: (1) there is no convolution layer, (2) it has a very wide coding layer with random untrained weights for sparse coding, and (3) it uses a learning rule for low interference learning with sparse coding. We demonstrate FlyOrien’s effectiveness in a dataset we modified for an object orientation task and a real-world robotic orientation task. Experiments show that FlyOrien is more efficient than traditional artificial neural networks, as it only needs a single epoch training to achieve Top-5 accuracy comparable to CNNs that typically converge after 100 epochs.

The paper is structured as follows: Section 2 introduces the details of the model, Section 3 pretenses the experiments, including experiments with a modified dataset (Section 3.1) and data from a robot in a real-world environment (Section 3.2).

2 MODEL

Our model, or FlyOrien, consists of two parts: a simplified MB model with firing-rate neurons and a modified associative learning rule, and a simplified CX modeled with a modified CANN. The former can learn the orientation of multiple objects, more specifically, associating a view of an object with an orientation angle. The latter merges multiple outputs of the former and provides a finer output. We also proposed a biologically plausible learning rule so that the MB model can learn images by only looking at them once.

For convenience of application, we simplified the MB and CX for a minimal model functioning in learning object orientation. It ignores neuron’s morphology, uses firing-rate neuron models instead of spiking neuron models, ignores dynamics inside neurons, and treats synapses between neurons as a linear mapping. However, there are still neural dynamics by neuron interactions in the simplified CX and synaptic plasticities by a biologically plausible learning rule from KCs to MBONs in the simplified MB.

2.1 SIMPLIFIED MUSHROOM BODY MODEL

The simplified MB has three layers including projection neurons (Figure 1b). The first layer consists of “PNs” conveying preprocessed images. The second layer consists of “KCs” encoding images. The third layer consists of “MBONs” outputting the likelihood of angles.

2.1.1 DATA PREPROCESSING

Insect sensory inputs are preprocessed before sending to KCs by PNs. The preprocessing can involve dimension reduction, noise reduction, normalization, and gain control (Gopfert & Robert, 2002). The actual preprocessing of visual signals in insects can be complex. The neural circuits in the optic lobe play an important role in processing vision in moving (Mauss et al., 2017), then visual information is projected to the MB by posterior lateral protocerebrum PNs (PLP-PNs) (Li et al., 2020c). Despite this, previous models suggest that the architecture of the mushroom body (MB) can process and learn from images without the need for complex feature extraction but directly on pixel-level information (Ardin et al., 2016; Dasgupta et al., 2017).

As a simple approximation to the optic lobe, which adjusts contrast through lateral inhibition, the first step of our model normalizes inputs. After normalization, the mean pixel intensity of each image is set to 0. The image is then flattened to allow for the model’s use across different modalities. Given a dataset (X, y) , where $X \in \mathbb{R}^{n \times d}$, each row represents a sample $\mathbf{x} \in \mathbb{R}^d$, n is the number of sample points, and d is the dimension of a sample point. A sample is shifted by the mean value \bar{x} of x before being passed to the PNs:

$$\hat{\mathbf{x}} = \mathbf{x} - \bar{x}, \quad (1)$$

where $\bar{x} = \sum_{i=0}^d x_i/d$, i is an index for the sample dimensions.

2.1.2 NETWORK ARCHITECTURE

FlyOrien uses a simplified PN-KC connection and WTA for encoding samples. The synaptic weights from PN to KC are noted as a matrix $W_{\text{PK}} \in \mathbb{R}^{q \times d}$, where q is the number of “KCs”. The elements of W_{PK} are random and binary, following a Bernoulli distribution, that is, $w_{\text{PK}ji} \sim \text{Bernoulli}(p)$, where j is the index of “KC” and $p = b/d$ is the probability of connection and b represents the expectation of how many “PNs” are connected to a “KC”. In our experiments, b is set to $0.1d$ so that $p = 0.1$. With W_{PK} , the input to “KCs” follows:

$$\mathbf{z} = W_{\text{PK}}\hat{\mathbf{x}}, \quad (2)$$

In the MB, the APL neuron induces lateral inhibition on KCs, allowing only the most strongly activated KCs to become active. FlyOrien approximates this WTA mechanism by keeping top h

activating “KCs” retain their output values, while others are set to zero:

$$\hat{z}_j = \begin{cases} z_j & \text{if } z_j \text{ is one of the } h \text{ largest entries in } \mathbf{z}_i \\ 0 & \text{otherwise} \end{cases} \quad (3)$$

where h directly controls the sparseness of the coding and j is a local index here for which “KC”. In our experiments, $h = 0.05q$. After WTA, the output of “KCs” is $\hat{\mathbf{z}} = (\hat{z}_1, \hat{z}_2, \dots, \hat{z}_j, \dots, \hat{z}_q) \in \mathbb{R}^q$.

Since a “KC” that is always active provides little useful information, we implemented a threshold to disable such “KCs”. The threshold we used is 0.25, meaning that if a “KC” remains active in more than one-quarter of the images, its output is always 0.

The synaptic weights from “KCs” to “MBONs” are presented as a matrix $W_{\text{KO}} \in \mathbb{R}^{m \times q}$, where m is the number of “MBONs”. The activities of “MBONs” are:

$$\hat{\mathbf{y}} = W_{\text{KO}} \hat{\mathbf{z}}, \quad (4)$$

The activity of each “MBON” is the likelihood of corresponding orientation given data sample \mathbf{x} .

2.1.3 LEARNING RULE

The MB is an associative learning center in insects. Associative learning is a type of classic conditioning that associates two stimuli or events. In the context of our model, the two stimuli are an image sample and the object orientation on the image. From an aspect of view in machine learning, we can interpret associative learning as supervised learning. Insects can continuously associate sensory stimuli with valences or behaviors, and the connections between KCs and MBONs play an important role in this process. In our model, learning occurs solely through adjusting the weights W_{KO} between these two layers.

We applied two variations of Hebbian rule (Hebb, 1949) for updating W_{KO} , which are referred to as Method 1 and 2, respectively. Method 1 treats learning as a progress to converge and adjusts a weight multiple times, while Method 2 treats the learning as an instant progress and a weight can only be adjusted once. In both methods, all weights between “KCs” and the “MBONs” are initialized to 0. During training, when an image \mathbf{x} and a label y is provided, \mathbf{x} is sparsely coded by the “KCs” as $\hat{\mathbf{z}}$, and y is presented by corresponding “MBONs” in a one-hot manner.

With a method 1, for each \mathbf{x} and y , every activating “KC” and the “MBON” connects according to the activity of the “KC”:

$$w_{\text{KO}kj} = \begin{cases} \alpha_{kj}(\hat{z}_j - w_{\text{KO}kj}) + w_{\text{KO}kj} & \text{if “MBON” } k \text{ is the label and “KC” } j \text{ activates,} \\ w_{\text{KO}kj} & \text{otherwise.} \end{cases} \quad (5)$$

where $w_{\text{KO}kj}$ is the weight from j th “KC” to k th “MBON”, α_{kj} is the learning rate, which typically starts from 1 and decays according to the rule $\alpha_{kj} = (1 - 10^{-4})\alpha_{kj}$ if the corresponding synapse is updated. Please note that weights from inactivating “KCs” are not updated. Learning ends when all images are looped once.

Different from Method 1, Method 2 updates W_{KO} in a binary manner. More specifically, for each \mathbf{x} and y , weights between activating “KCs” and the corresponding “MBON” are set to 1.

$$w_{\text{KO}kj} = \begin{cases} 1 & \text{if “MBON” } k \text{ is the label and “KC” } j \text{ activates,} \\ w_{\text{KO}kj} & \text{otherwise.} \end{cases} \quad (6)$$

Hence, there is no mechanism to weaken weights in Method 2. In other words, there is no forgetting on a synaptic level.

The output of the above half model is the likelihood of multi-class labels. This part of the model was evaluated in the experiment with and without the second half.

2.2 CANN WITH MULTIPLE INPUTS

Unlike a typical multi-class classification dataset where there are no correlations between labels, our dataset exhibits correlations between labels, allowing outputs from “MBONs” to be interpolated for finer orientation resolution. As reviewed in the introduction, in insects, multiple MBONs nerves to

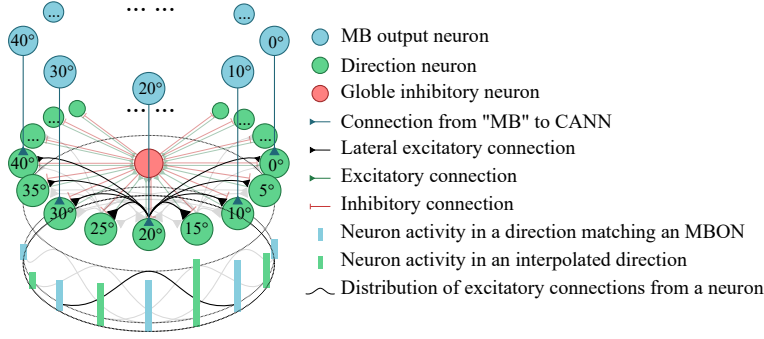


Figure 2: In our model, the continuous Attractor Neural Network (CANN) is functional as a lower-pass spatial filter and interpolator of the “MB” outputs. The “MB” outputs are fed to corresponding neurons in the CANN, which has neurons representing finer directions. The neurons, their lateral excitatory connections, and global inhibitory connections form a ring attractor together.

the fan-shaped body in the CX. As CANN has been proved to be a simplified model of CX, we built the second half of FlyOrien by modifying CANN to receive multiple outputs from “MBONs”(Fig 2).

The CANN for CX describes a ring attractor by multiple interconnected neurons. Every neuron is allocated with an orientation, stimulates neurons nearby and inhibits all neurons. Their input dynamics is denoted as $U(o, t)$ and described based on the orientation o instead explicitly by neurons:

$$\tau \frac{\partial U(o, t)}{\partial t} = -U(o, t) + \rho \int_{x'} J(o, o') r(o', t) dx' + I^{ext}(o, t) \quad (7)$$

Where τ is the time constant for the population dynamics, which is on the order of 1ms (Gutkin et al., 2003), $\rho = h/(2\pi)$ is the neural density and h is the number that orientation is discretized, $I^{ext}(o, t)$ is the input to the neuron at o at time t . $J(o, o') = \frac{J_0}{\sqrt{2\pi}a} \exp(-|o - o'|^2/2a^2)$ presents the excitatory connections from the neuron at o' to the neuron at o , where $a = 0.1$ is the half-width of the range of excitatory connections. $r(o, t)$ is the firing rate of neurons:

$$r(o, t) = \frac{U(o, t)^2}{1 + k\rho \int U(o', t)^2 do'} \quad (8)$$

where $k = 0.1$ is the degree of the inhibition. The contribution of inhibitory connection is achieved indirectly through the divisive normalization in equation 8.

The output of the simplified MB model is fed to the CANN by the term $I^{ext}(o, t)$, where o corresponds to the labels of “MBONs”. As shown in Fig 2, there are more neurons in CANN than MBONs for finer directions, and each MBON outputs to a corresponding neuron for the same direction. Thus with the dynamics of CANN, CANN can integrate information from multiple outputs from the “MBONs”, and predict finer orientations.

Thus, we can add more neurons in CANN to interpolate for a finer resolution output. The model is implemented with Python and attached in supplementary material.

3 EXPERIMENTS

We tested the model on a dataset for object orientation learning and a dataset from a robot for real-world evaluation. There are two types of tasks: retrieval and prediction. Please note the retrieval task tests the ability of the models to associate images with their corresponding orientations, thus the same images are presented in the test. Computation is conducted on a desktop workstation with the 12th Gen Intel® Core™i7-12700 Processor, 32GB RAM, and the NVIDIA® GeForce RTX™3090. We compared our model with typical convolutional neural networks (CNNs) in object orientation retrieving and prediction, and our model trained on CPU can even achieve better performance 7 to 45 times faster in training time than CNNs trained in GPU.



Figure 3: Example samples from COIL-100-O (Top) and COIL-100-AS (Bottom).

3.1 OBJECT ORIENTATIONS LEARNING IN COIL DATASET

Our model was evaluated on a dataset modified from COIL-100 dataset (Nene et al., 1996) along with baseline models. The original dataset contains 100 objects captured at 72 different orientations and in total 7200 images which are labeled with the object. The size of the original image is 128×128 , for each of the images, there are $128 \times 128 \times 3 = 49152$ channels of values as the image is RGB colored. We modified the dataset by associating the images with object orientation instead of the object. Thus, different objects can be associated with the same label, while the same objects are labeled differently, and there is strong interference while a model is trained on this modified dataset.

Because there is no correlation between samples with the same label in this dataset, cross-validation is unsuitable for this task. This is a key distinction from typical datasets. In most classification tasks, samples with the same label share similar features, allowing for knowledge generalization across those samples. However, this is not the case in our dataset. Since samples with the same label are not correlated, cross-validation, which typically evaluates generalization within samples of the same label, becomes less meaningful. As we will show later, both baseline models and our proposed model have achieved near-zero accuracy with cross-validation (Figure A3, Table A6).

We divided this dataset into two groups according to whether the object is axisymmetric and without a textured pattern, resulting in COIL-100-Ordinary(COIL-100-O) group and COIL-100-Axisymmetric(COIL-100-AS) group. For COIL-100-O, the objects are not axisymmetric or have clear textured patterns. For COIL-100-AS, the objects are axisymmetric without views of a clear textured pattern. In COIL-100-AS, different views of the same object are so similar that human eyes cannot even distinguish them. We present views of two objects (Figure 3), the first row is from COIL-100-O, and the second row is from COIL-100-AS.

3.1.1 RETRIEVAL TASK BY THE SIMPLIFIED MB

The first experiment on COIL is the retrieval of object orientation. This experiment does not discriminate between the training set and the testing set. Instead, the model should retrieve the angle of objects in the previously viewed image. It is conceptually simple, but because the same object shares the same features but has different labels for orientation, there is interference when a typical ANN learns the orientations. The Top-5 criterion is applied to retrieval accuracy. That is, if the correct label is in the Top-5 predicted labels by a model, this model predicts correctly.

In training, the learning rules proposed in Section 2.1.3 were applied to our model. With the learning rule, our model only loops through the dataset once. Differently, baseline models were trained for 200 epochs. They were optimized with the Adam optimizer implemented in PyTorch with default parameters. The loss function for gradient descent was cross entropy provided by PyTorch with default parameters.

More KCs, more accurate. We evaluated the influence of the number of active KCs on retrieval accuracy. As the number of KCs increases, the accuracy of our methods improves across both datasets, approaching convergence when the number of KCs is close to 10,000 (Figure 4).

Retrieval accuracy of the simplified MB As our model’s performance converges around 10,000 KCs, we used models with 10,240 KCs for comparison with the baselines. This choice is in favor of common multiples of powers of 2 and 10 and also aligns with biological plausibility (Abdelrahman et al., 2021). Figure A1 and A2 show the Top-5 active MBONs for every object in an example

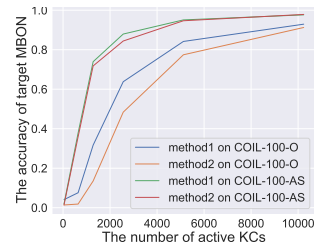


Figure 4: Accuracy with different number of KCs.

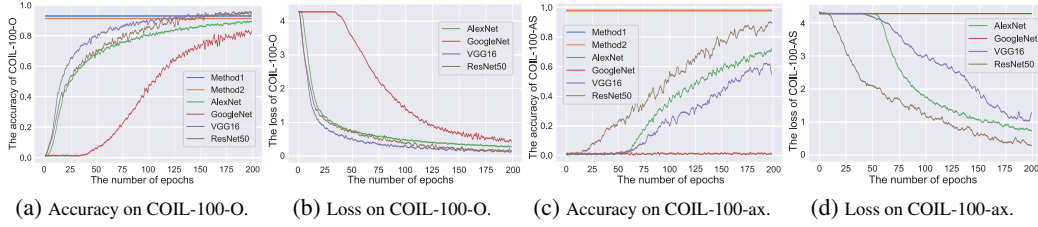


Figure 5: Accuracy and loss in the retrieval task on COIL-100-O and COIL-100-ax.

orientation in COIL. The first column is an example orientation, the second column is the corresponding Top-5 MBONs with weights learned by method 1, and the third column shows the results from method 2. FlyOrien achieves more than 90% accuracy across both datasets in retrieving the orientation of a viewed object after a single learning instance.

Baselines take much longer training time for the same performance. We compared the accuracy, training time, and incremental learning ability of our two methods with CNNs like AlexNet (Krizhevsky et al., 2012), GoogleNet (Szegedy et al., 2015), VGG16 (Simonyan & Zisserman, 2014), ResNet50 (He et al., 2016), as illustrated in Table 1. The accuracy and loss change of increasing epochs for the baselines is shown in Figure 5. In Figure 5a and 5c, our methods are displayed as horizontal lines because they only need to be learned once. Other models take 1.6 to 80.6 times longer for a similar performance. Please note that we did not accelerate our model on GPU.

Table 1: Retrieval accuracy (%) and training time (s) of the simplified MB and baselines.

Method	Platform	COIL-100-O		COIL-100-AS	
		Acc	Time	Acc	Time
Method 1	CPU	92.93	112	97.65	47
Method 2	CPU	91.26	61	97.86	47
AlexNet	GPU	97.77	873	86.22	131
GoogleNet	GPU	92.77	1845	35.01	273
VGG16	GPU	97.91	10390	71.05	1537
ResNet50	GPU	97.92	4317	95.30	639
MobileNet	GPU	99.89	947	79.81	166
ShuffleNet	GPU	99.51	1651	83.55	289

Incremental learning ability We trained FlyOrien incrementally and calculated accuracy on previously trained objects to assess the model’s incremental learning ability. Specifically, after training on all images of an object, we evaluate the model’s accuracy on every object that has been learned. The results, shown in Appendix Figures A4 to A5, indicate that our model can acquire new knowledge without forgetting previously learned knowledge, even for axisymmetric objects that are challenging for humans. Appendix Figure A6 shows the results in the dimension of time along with results by baseline models in an incremental learning setup. It demonstrates that while all baseline models experience catastrophic forgetting over 10 iterations of optimization, our model is nearly unaffected by the trained order of samples.

3.1.2 PREDICTION ACCURACY OF THE SIMPLIFIED MB AND CX

The first half of FlyOrien outputs label likelihoods in a multi-class classification setup. However, for real-world applications, we aim for more precise predictions. This experiment evaluates the capability of the full FlyOrien model, combined with CANN, to predict orientations with a finer resolution than that used in training. For ease of evaluation, we divided the data based on object orientations, with 72 evenly distributed orientations, alternating between the training and testing sets.

For a fair comparison, we also integrated the baseline models with CANN, resulting in two setups: models with and without CANN. In the first setup, without CANN, orientations in the testing set cannot be predicted directly, so the adjacent angle is used as the correct prediction criterion. In the second setup, although the baseline models only predict orientations in the testing set, with

CANN, the orientations in the training set can be predicted, so the Top-5 criterion for multi-class classification is applied. It is important to note that the evaluation criteria differ between these two setups, and comparisons are valid only within the same setup.

With the first setup and Method 2, the simplified MB in our model outperforms baselines (Table 2, second and third rows). The accuracy of the simplified MB is 95.34% on the testing set while the best baseline is AlexNet with 91.28% accuracy. With the second setup and Method 2, the simplified MB with CANN, or the full FlyOrien model, has the highest training accuracy 98.95%, while not best for testing accuracy, 66.57%. A possible reason is that the simplified MB tends to output a bimodal distribution, and there is a second set of large likelihood peaks on the opposite side of the orientation, which moves the peak of CANN away from the correct orientation.

Table 2: Accuracy (%) of FlyOrien and four baselines.

Model	Original Model		Original Model + CANN	
	Training	Testing	Training	Testing
Simplified MB	98.86	95.34	98.95	66.57
AlexNet	92.27	91.28	83.88	20.34
GoogleNet	11.59	2.78	3.35	5.56
VGG16	94.41	90.84	90.33	81.45
ResNet50	94.06	90.94	85.82	81.96
MobileNet	95.09	94.44	78.21	77.56
Shufflenet	71.37	79.06	55.77	54.49

We also evaluated the training accuracy and testing accuracy of our model and baseline models on the COIL-100-O dataset with altered contrast in images. For more details, see Section A.2.5.

3.2 DETECTION ACCURACY ON REAL OBJECTS COLLECTED BY A QUADRUPED ROBOT

To simulate an animal finding directions, two experiments were conducted on a quadruped robot. In experiment 1, the robot finds a familiar object or landmark in the environment and makes an angle judgment around the landmark 360° . In the second experiment, in the empty scene with no suitable objects or landmarks to be surrounded, the angle is according to its own orientation. Each sample collected a total of 360 images, with each image size of 128×128 pixels. Compared with the test of re-designed datasets, the angle interval of the testing set of this experiment has changed from 10° to 1° , which is more dense and more consistent with the randomness of the angle and position of the robot in the real scene.



Figure 6: A quadruped robot looks at a landmark.

Object’s orientation by vision from robot

In this experiment, a robot motion control and image sampling algorithm was designed to realize the robot sampling from different angles during the 360° rotation around the object (Figure6). The robot rotates around an object, taking one photo per degree with its head camera, for a total of 360 photos. The binocular fisheye cameras on the robot’s head have a 180° field of view. Through the official camera calibration algorithm built into the robot, the corrected photos are transmitted in real time during the sampling process. The image from both the left and right eyes is 800×928 . We will extract the image from the left eye for use in the subsequent experiment, compressing it to 128×128 .

The photos of every ten degrees are selected as the training data set, the rest are taken as the testing set, and the nearest ten degrees are taken as the label for the accuracy test. Cups, foam boxes, and plants were sampled and tested for accuracy. The uncropped data sets were also tested (Figure7). It can be observed that the robot’s Top-5 object orientation accuracy is over 96%, and the Top-2 accuracy is over 80% (Table 3). The performance remains relatively stable on the dense testing set with 1° intervals.

Robot’s orientation by vision to the environment

In this experiment, the robot can rotate in circles only by setting rotational speed. The robot was made to rotate itself once for sampling in three different scenes: lab 1, lab 2, and corridor(Fig.8).

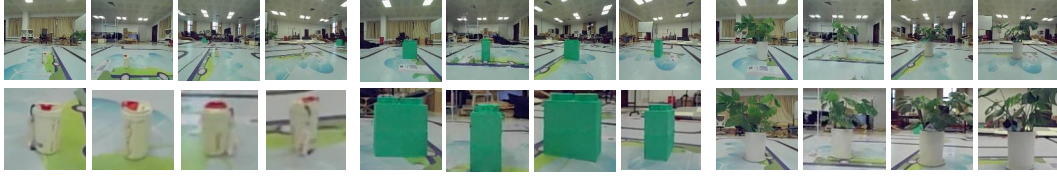


Figure 7: Sampled images of a cup, a foam box, and a plant at 0° , 90° , 180° , and 270° (Top: original view from the robot, Bottom: cropped view on objects for orientation.)

Table 3: Accuracy of network trained with a single data set.

Object	cup	foam box	plant	cup (in scene)	foam box (in scene)	plant (in scene)
acc(Top-2)	80.56	82.93	83.33	88.89	87.83	91.11
acc(Top-5)	97.78	97.56	96.67	98.89	97.72	98.89

The sampling method is the same as in the previous experiment. The robot achieved an orientation accuracy of over 96% when choosing Top-5 activated MBONs, and over 80% when choosing Top-2 activated MBONs (Table 4). The performance remains relatively stable on the dense testing set with 1° intervals.

Training network testing on complex data sets

The six image datasets from the Object’s orientation experiments were combined into Dataset 1. The three image datasets from the Robot’s orientation experiments were combined into Dataset 2. Finally, Dataset 1 and Dataset 2 were merged into Dataset 3 to test the neural network’s stability in long-term learning. By comparing Table 5 with Tables 3 and 4, and by comparing Dataset 3 with Dataset 1 and Dataset 2, it can be observed that the accuracy of neural network was not significantly affected by the change in the data set from single to complex. This indicates that the neural network has good stability for long-term learning.

4 DISCUSSION AND CONCLUSION

Inspired by the neural circuits of insects, particularly the MB and CX, we proposed FlyOrien, a bio-inspired model for incremental learning of object orientation. The model mimics the MB’s sparse coding and associative learning while utilizing the CX to integrate multiple sensory inputs to refine orientation detection. FlyOrien is designed to learn object orientations efficiently after a single exposure, and because it mimics the sparse coding of MB, it has the potential to generalize to multimodal inputs, such as posture, olfactory, and directional cues, which will be investigated in further research.

FlyOrien was tested on open-source datasets and real-world robotic tasks, demonstrating strong performance in estimating object orientations and handling ego motion in complex scenes. Its ability to learn incrementally, without large datasets or extensive training, highlights its suitability for real-time applications.

Without relying on convolutional layers, FlyOrien learns object orientation efficiently without catastrophic forgetting, benefiting from its large number of pattern detectors and sparse coding. For instance, samples in COIL-100-AS with the same label are very similar, so subtle features, such as specific patterns, are crucial for orientation detection, but CNNs are not optimized for this. CNNs generalize by learning from fewer images and using shared weights to capture relationships between local features. Convolutional kernels in the first layer detect low-level features, but this generaliza-



Figure 8: Sampling images of lab1, lab2, and corridor at 0° , 90° , 180° , and 270°

Scene	lab1	lab2	corridor	Original Method	dataset 1	dataset 2	dataset 3
acc(Top-2)	91.41	87.52	83.17	acc(Top-2)	77.31	79.72	79.14
acc(Top-5)	98.53	99.31	93.32	acc(Top-5)	96.00	88.98	95.13

Table 4: Accuracy on a single dataset

Table 5: Accuracy on a complex situation

tion can overshadow rare or unique patterns, risking them being forgotten. In contrast, MB-like architectures excel at identifying these subtle features and preventing forgetting by maintaining fixed connections after learning. In our model, many “KCs,” each connected to only a few pixels, act as specialized pattern detectors. Unlike CNNs, which apply the same filters across regions, FlyOrien uses more filters simultaneously, detecting intricate details in a single pass. This key difference enables FlyOrien to perform better and learn faster in our tasks.

While FlyOrien offers significant benefits, it is sensitive to pixel-level changes, affecting performance when objects deform or lighting varies. Addressing these limitations is a key area for future research, particularly by incorporating the optic lobe which is crucial for dynamic vision processing. Extending the CX model to a two-dimensional CANN could also improve navigation in complex, unmapped environments, enhancing FlyOrien’s robustness for more sophisticated spatial tasks.

FlyOrien’s lightweight design, free from GPU dependence, allows it to run effectively on small devices like drones and robots, making it ideal for resource-constrained tasks like object tracking, navigation, and surveillance, where low power consumption and computational efficiency are critical.

In practical applications, FlyOrien presents minimal risks. Its use in autonomous robots can improve navigation and object recognition without needing extensive computational resources. However, ensuring transparency and human oversight in deployment is crucial. When used for navigation or surveillance in public spaces, it’s important to respect privacy and operate within ethical guidelines. FlyOrien’s efficiency on small robots makes it ideal for search and rescue, environmental monitoring, and industrial automation. With safeguards in place, FlyOrien can positively contribute to these fields without significant risks.

REFERENCES

- Nada Y Abdelrahman, Eleni Vasilaki, and Andrew C Lin. Compensatory variability in network parameters enhances memory performance in the drosophila mushroom body. *Proceedings of the National Academy of Sciences*, 118(49):e2102158118, 2021.
- Paul Ardin, Fei Peng, Michael Mangan, Konstantinos Lagogiannis, and Barbara Webb. Using an insect mushroom body circuit to encode route memory in complex natural environments. *PLoS computational biology*, 12(2):e1004683, 2016.
- Yoshinori Aso, Divya Sitaraman, Toshiharu Ichinose, Karla R Kaun, Katrin Vogt, Ghislain Belliard-Guérin, Pierre-Yves Plaçais, Alice A Robie, Nobuhiro Yamagata, Christopher Schnaitmann, et al. Mushroom body output neurons encode valence and guide memory-based action selection in drosophila. *elife*, 3:e04580, 2014.
- Lothar Baltruschat, Luigi Prisco, Philipp Ranft, J. Scott Lauritzen, André Fiala, Davi D. Bock, and Gaia Tavosanis. Circuit reorganization in the Drosophila mushroom body calyx accompanies memory consolidation. *Cell Reports*, 34(11), mar 2021. ISSN 22111247. doi: 10.1016/j.celrep.2021.108871. URL <https://doi.org/10.1016/j.celrep.2021.108871>.
- James E.M. Bennett, Andrew Philippides, and Thomas Nowotny. Learning with reinforcement prediction errors in a model of the Drosophila mushroom body. *Nature Communications*, 12(1): 1–14, may 2021. ISSN 20411723. doi: 10.1038/s41467-021-22592-4. URL <https://www.nature.com/articles/s41467-021-22592-4>.
- Sophie JC Caron, Vanessa Ruta, Larry F Abbott, and Richard Axel. Random convergence of olfactory inputs in the drosophila mushroom body. *Nature*, 497(7447):113–117, 2013.
- Sanjoy Dasgupta, Charles F Stevens, and Saket Navlakha. A neural algorithm for a fundamental computing problem. *Science*, 358(6364):793–796, 2017.

- Zhaoxin Fan, Yazhi Zhu, Yulin He, Qi Sun, Hongyan Liu, and Jun He. Deep learning on monocular object pose detection and tracking: A comprehensive overview. *ACM Computing Surveys*, 55(4): 1–40, 2022.
- Romain Franconville, Celia Beron, and Vivek Jayaraman. Building a functional connectome of the drosophila central complex. *eLife*, 7:1–24, 2018. ISSN 2050084X. doi: 10.7554/eLife.37017.
- Ishani Ganguly, Emily L. Heckman, Ashok Litwin-Kumar, E. Josephine Clowney, and Rudy Behnia. Diversity of visual inputs to Kenyon cells of the *Drosophila* mushroom body. *Nature Communications*, 15(1), 2024. ISSN 20411723. doi: 10.1038/s41467-024-49616-z. URL <http://dx.doi.org/10.1038/s41467-024-49616-z>.
- Aristides Gionis, Piotr Indyk, Rajeev Motwani, et al. Similarity search in high dimensions via hashing. In *Vldb*, volume 99, pp. 518–529, 1999.
- Martin C Gopfert and Daniel Robert. The mechanical basis of drosophila audition. *Journal of Experimental Biology*, 205(9):1199–1208, 2002.
- Boris Gutkin, David Pinto, and Bard Ermentrout. Mathematical neuroscience: from neurons to circuits to systems. *Journal of Physiology-Paris*, 97(2-3):209–219, 2003.
- Elissa A Hallem and John R Carlson. Coding of odors by a receptor repertoire. *Cell*, 125(1): 143–160, 2006.
- Jiaming Han, Jian Ding, Nan Xue, and Gui-Song Xia. Redet: A rotation-equivariant detector for aerial object detection. In *Proceedings of the IEEE/CVF conference on computer vision and pattern recognition*, pp. 2786–2795, 2021.
- Tatsuya Tatz Hayashi, Alexander John MacKenzie, Ishani Ganguly, Kaitlyn Elizabeth Ellis, Hayley Marie Smihula, Miles Solomon Jacob, Ashok Litwin-Kumar, and Sophie Jeanne Cécile Caron. Mushroom body input connections form independently of sensory activity in *Drosophila melanogaster*. *Current Biology*, 32(18):4000–4012.e5, 2022. ISSN 18790445. doi: 10.1016/j.cub.2022.07.055.
- Kaiming He, Xiangyu Zhang, Shaoqing Ren, and Jian Sun. Deep residual learning for image recognition. In *Proceedings of the IEEE conference on computer vision and pattern recognition*, pp. 770–778, 2016.
- D O Hebb. *The organization of behavior; a neuropsychological theory*. Wiley, Oxford, England, 1949.
- Stanley Heinze. Unraveling the neural basis of insect navigation. *Current Opinion in Insect Science*, 24(September 2017):58–67, 2017. ISSN 22145753. doi: 10.1016/j.cois.2017.09.001.
- Anna Honkanen, Andrea Adden, Josiane Da Silva Freitas, and Stanley Heinze. The insect central complex and the neural basis of navigational strategies. *Journal of Experimental Biology*, 222(Pt Suppl 1), feb 2019. ISSN 00220949. doi: 10.1242/jeb.188854. URL www.insectbraindb.org; https://journals.biologists.com/jeb/article/222/Suppl_1/jeb188854/2882/The-insect-central-complex-and-the-neural-basis-of <http://www.ncbi.nlm.nih.gov/pubmed/30728235> <http://www.pubmedcentral.nih.gov/articlerender.fcgi?artid=PMC64744>.
- Kate J Jeffery, Hector JI Page, and Simon M Stringer. Optimal cue combination and landmark-stability learning in the head direction system. *The Journal of physiology*, 594(22):6527–6534, 2016.
- Alex Krizhevsky, Ilya Sutskever, and Geoffrey E Hinton. Imagenet classification with deep convolutional neural networks. *Advances in neural information processing systems*, 25, 2012.

- Feng Li, Jack Lindsey, Elizabeth C Marin, Nils Otto, Marisa Dreher, Georgia Dempsey, Ildiko Stark, Alexander Shakeel Bates, Markus William Pleijzier, Philipp Schlegel, Aljoscha Nern, Shinya Takemura, Nils Eckstein, Tansy Yang, Audrey Francis, Amalia Braun, Ruchi Parekh, Marta Costa, Louis Scheffer, Yoshinori Aso, Gregory SXE Jefferis, Larry F Abbott, Ashok Litwin-Kumar, Scott Waddell, and Gerald M Rubin. The connectome of the adult drosophila mushroom body provides insights into function. *eLife*, 9:1–217, dec 2020a. ISSN 2050084X. doi: 10.7554/eLife.62576. URL <https://elifesciences.org/articles/62576>.
- Feng Li, Jack W Lindsey, Elizabeth C Marin, Nils Otto, Marisa Dreher, Georgia Dempsey, Ildiko Stark, Alexander S Bates, Markus William Pleijzier, Philipp Schlegel, et al. The connectome of the adult drosophila mushroom body provides insights into function. *Elife*, 9:e62576, 2020b.
- Jinzh Li, Brennan Dale Mahoney, Miles Solomon Jacob, and Sophie Jeanne Cécile Caron. Visual Input into the Drosophila melanogaster Mushroom Body. *Cell Reports*, 32(11), 2020c. ISSN 22111247. doi: 10.1016/j.celrep.2020.108138.
- Jianqi Ma, Weiyuan Shao, Hao Ye, Li Wang, Hong Wang, Yingbin Zheng, and Xiangyang Xue. Arbitrary-oriented scene text detection via rotation proposals. *IEEE transactions on multimedia*, 20(11):3111–3122, 2018.
- Alex S. Mauss, Anna Vlasits, Alexander Borst, and Marla Feller. Visual Circuits for Direction Selectivity. *Annual Review of Neuroscience*, 40:211–230, 2017. ISSN 15454126. doi: 10.1146/annurev-neuro-072116-031335.
- Qi Ming, Lingjuan Miao, Zhiqiang Zhou, Junjie Song, Yunpeng Dong, and Xue Yang. Task interleaving and orientation estimation for high-precision oriented object detection in aerial images. *ISPRS Journal of Photogrammetry and Remote Sensing*, 196:241–255, 2023.
- Mehrab N. Modi, Yichun Shuai, and Glenn C. Turner. The Drosophila Mushroom Body: From Architecture to Algorithm in a Learning Circuit. *Annual Review of Neuroscience*, 43:465–484, 2020. ISSN 15454126. doi: 10.1146/annurev-neuro-080317-0621333.
- Sameer A Nene, Shree K Nayar, Hiroshi Murase, et al. Columbia object image library (coil-20). 1996.
- Shawn R Olsen, Vikas Bhandawat, and Rachel I Wilson. Divisive normalization in olfactory population codes. *Neuron*, 66(2):287–299, 2010.
- Edwin Olson. AprilTag: A robust and flexible visual fiducial system. *Proceedings - IEEE International Conference on Robotics and Automation*, pp. 3400–3407, 2011. ISSN 10504729. doi: 10.1109/ICRA.2011.5979561.
- John M Pearce and Mark E Bouton. Theories of associative learning in animals. *Annual review of psychology*, 52(1):111–139, 2001.
- Karen Simonyan and Andrew Zisserman. Very deep convolutional networks for large-scale image recognition. *arXiv preprint arXiv:1409.1556*, 2014.
- Darren Smith, Jan Wessnitzer, and Barbara Webb. A model of associative learning in the mushroom body. *Biological Cybernetics*, 99(2):89–103, 2008. ISSN 03401200. doi: 10.1007/s00422-008-0241-1.
- Charles F Stevens. A statistical property of fly odor responses is conserved across odors. *Proceedings of the National Academy of Sciences*, 113(24):6737–6742, 2016.
- Thomas Stone, Barbara Webb, Andrea Adden, Nicolai Ben Weddig, Anna Honkanen, Rachel Templin, William Wcislo, Luca Scimeca, Eric Warrant, and Stanley Heinze. An Anatomically Constrained Model for Path Integration in the Bee Brain. *Current Biology*, 27(20):3069–3085.e11, 2017. ISSN 09609822. doi: 10.1016/j.cub.2017.08.052.
- Christian Szegedy, Wei Liu, Yangqing Jia, Pierre Sermanet, Scott Reed, Dragomir Anguelov, Dumitru Erhan, Vincent Vanhoucke, and Andrew Rabinovich. Going deeper with convolutions. In *Proceedings of the IEEE conference on computer vision and pattern recognition*, pp. 1–9, 2015.

- Gido M Van de Ven, Tinne Tuytelaars, and Andreas S Tolias. Three types of incremental learning. *Nature Machine Intelligence*, 4(12):1185–1197, 2022.
- Barbara Webb and Antoine Wystrach. Neural mechanisms of insect navigation. *Current Opinion in Insect Science*, 15:27–39, 2016.
- Tianqi Wei, Rana Alkhoury Maroun, Qinghai Guo, and Barbara Webb. Devfly: Bio-inspired development of binary connections for locality preserving sparse codes. *Advances in Neural Information Processing Systems*, 35:2320–2332, 2022.
- Jan Wessnitzer, Barbara Webb, and Darren Smith. A model of non-elemental associative learning in the mushroom body neuropil of the insect brain. *Lecture Notes in Computer Science (including subseries Lecture Notes in Artificial Intelligence and Lecture Notes in Bioinformatics)*, 4431 LNCS(PART 1):488–497, 2007. ISSN 16113349. doi: 10.1007/978-3-540-71618-1_54.
- Hongjin Wu, Ruoshan Lei, and Yibing Peng. Pcbnet: A lightweight convolutional neural network for defect inspection in surface mount technology. *IEEE Transactions on Instrumentation and Measurement*, 71:1–14, 2022.
- Si Wu, KY Michael Wong, CC Alan Fung, Yuanyuan Mi, and Wenhao Zhang. Continuous attractor neural networks: candidate of a canonical model for neural information representation. *F1000Research*, 5, 2016.
- Gui-Song Xia, Xiang Bai, Jian Ding, Zhen Zhu, Serge Belongie, Jiebo Luo, Mihai Datcu, Marcello Pelillo, and Liangpei Zhang. Dota: A large-scale dataset for object detection in aerial images. In *Proceedings of the IEEE conference on computer vision and pattern recognition*, pp. 3974–3983, 2018.
- Yi Yu and Feipeng Da. Phase-shifting coder: Predicting accurate orientation in oriented object detection. In *Proceedings of the IEEE/CVF Conference on Computer Vision and Pattern Recognition*, pp. 13354–13363, 2023.
- Kechen Zhang. Representation of spatial orientation by the intrinsic dynamics of the head-direction cell ensemble: a theory. *Journal of Neuroscience*, 16(6):2112–2126, 1996.
- Zhihao Zheng, Feng Li, Corey Fisher, Iqbal J Ali, Nadiya Sharifi, Steven Calle-Schuler, Joseph Hsu, Najla Masoodpanah, Lucia Kmecova, Tom Kazimiers, et al. Structured sampling of olfactory input by the fly mushroom body. *Current Biology*, 32(15):3334–3349, 2022.
- Le Zhu, Michael Mangan, and Barbara Webb. Spatio-Temporal Memory for Navigation in a Mushroom Body Model. In *Biomimetic and Biohybrid Systems*, volume 12413, pp. 415–426. Springer International Publishing, 2020. ISBN 978-3-030-64313-3. doi: 10.1007/978-3-030-64313-3_39. URL http://link.springer.com/10.1007/978-3-030-64313-3_39.

A APPENDIX

A.1 ALGORITHM

A.1.1 ALGORITHM FOR DATA PREPROCESSING AND NETWORK ARCHITECTURE

Algorithm 1 Data Preprocessing and Network Architecture in the simplified MB

```

1: Input: Dataset  $(X, y)$  where  $X \in \mathbb{R}^{n \times d}$ 
2: Output: Activation of “MBONs”  $\hat{\mathbf{z}}$  for labels’ likelihood
3: Initialize weights  $W_{PK} \in \mathbb{R}^{q \times d}$ ,  $w_{PKji} \sim \text{Bernoulli}(p)$ 
4: Initialize “KCs” activation mask:  $\mathbf{v} = \mathbf{1}$ 
5: Initialize weights  $W_{KO} \in \mathbb{R}^{m \times q}$ 
6: // Step 1: Normalize Inputs
7: for each sample  $\mathbf{x} \in X$  do
8:   Compute mean  $\bar{x} = \frac{1}{d} \sum_{j=1}^d x_j$ 
9:   Shift the sample:  $\hat{\mathbf{x}} = \mathbf{x} - \bar{x}$ 
10: end for
11: for each sample  $\mathbf{x} \in X$  do
12:   // Step 2: Activation and outputs of “KCs”
13:   Compute “KCs” activation:  $\mathbf{z} = W_{PK}\hat{\mathbf{x}}$ 
14:   Keep top  $h$  activating KCs, whose indexes are entries of  $\mathbf{u}$ 
15:   for each  $j \in \mathbf{u}$  do
16:     if  $z_j$  is one of the  $h$  largest entries in  $\mathbf{z}$  then
17:        $\hat{z}_j = z_j v_j$ 
18:     else
19:        $\hat{z}_j = 0$ 
20:     end if
21:   end for
22:   // Step 3: Optionally disable over-activating “KCs”
23:   for each  $j \in \mathbf{u}$  do
24:     if KC  $j$  response to more than 1/4 samples then
25:        $v_j = 0$ 
26:     end if
27:   end for
28:   // Step 4: Activation and outputs of “MBONs”
29:   Compute “MBONs” activities:  $\hat{\mathbf{y}} = W_{KO}\hat{\mathbf{z}}$ 
30:   // Step 5: Learning Rule
31:   Method 1: Hebbian Learning with continuous Weights
32:   for each active KC  $j$  do
33:     if  $k$  is the label  $y$  then
34:       Update weights:  $w_{KOkj} \leftarrow \alpha(\hat{z}_j - w_{KOkj}) + w_{KOkj}$ 
35:     end if
36:   end for
37:   Decay learning rate:  $\alpha \leftarrow (1 - 10^{-4})\alpha$ 
38:   Method 2: Hebbian Learning with Binary Weights
39:   for each active KC  $j$  do
40:     if  $k$  is the label  $y$  then
41:       Set weight:  $w_{KOkj} \leftarrow 1$ 
42:     end if
43:   end for
44: end for

```

A.2 EXPERIMENTS

A.2.1 TOP-5 ACTIVE MBONs FOR THE WHOLE DATASET

Object	Original angle	Top5 active MBONs(method1)	Top5 active MBONs(method2)	Object	Original angle	Top5 active MBONs(method1)	Top5 active MBONs(method2)
	45	45, 30, 40, 25, 215	45, 30, 25, 40, 215		310	310, 315, 320, 120, 305	310, 315, 320, 120, 305
	30	30, 35, 25, 20, 40	30, 35, 40, 20, 25		255	255,265,260,270,275	255,265,275,260,160
	115	115, 110, 145, 255, 180	115, 145, 150, 110, 255		220	220,215,225,230,210	220,215,225,230,210
	75	75, 80, 70, 310, 85	75, 80, 310, 70, 85		50	50,55,45,65,60	50,55,65,45,40
	225	225, 45, 40, 220, 35	225, 40, 45, 35, 220		165	165,185,195,160,170	165,185,195,170,160
	25	25, 20, 10,15, 30	425, 20, 10, 15, 35		230	230, 255, 250, 225, 0	125, 215, 225, 230, 250
	80	80, 75, 85, 90, 70	80, 75, 85, 90, 95		190	190, 195, 200, 180, 205	190, 195, 200, 180, 170
	160	160, 165, 155, 185, 150	160, 150, 155, 165, 185		170	170, 165, 160, 175, 155	170, 165, 160, 145, 155
	165	165, 190, 170, 160, 195	165, 190, 170, 160, 200		25	20, 15, 25, 30, 10	20, 15, 25, 30, 10
	130	130, 135, 140, 125, 120	130, 135, 125, 140, 120		215	215, 210, 50, 220, 90	210, 215, 290, 230, 265
	220	220, 215, 225, 230, 210	220, 215, 225, 230, 210		25	25, 10, 30, 20, 5	25, 10, 30, 20, 5
	205	205, 245, 215, 70, 220	205, 215, 245, 200, 220		190	190, 185, 195, 210, 175	185, 190, 205, 210, 195
	60	60, 65, 55, 40, 15	60, 65, 55, 40, 15		155	155, 175, 160, 145, 170	155, 175, 145, 170, 160
	45	45, 40, 50, 35, 30	45, 40, 50, 35, 55		25	25, 10, 30, 5, 20	25, 10, 30, 20, 5
	170	170,175, 165, 180, 185	170, 175, 165, 180, 185		145	145, 150, 140, 135, 130	145, 150, 140, 320, 130
	15	15, 10, 5, 20, 0	15, 10, 5, 20, 0		55	55, 60, 70, 85, 80	55, 60, 70, 85, 40
	210	210, 205, 200, 215, 195	210, 205, 200, 195, 215		125	125, 120, 115, 130, 135	125, 120, 115, 130, 135
	175	175, 170, 180, 165, 160	175, 180, 170, 165, 185		185	185, 180, 190, 165, 175	185, 180, 190, 165, 175
	260	260, 265, 250, 255, 280	260, 250, 265, 285, 290		170	170, 175, 165, 180, 0	170, 175, 165, 180, 185
	0	0, 5, 10, 50, 15	0, 5, 10, 15, 50		35	35, 20, 30, 25, 40	35, 20, 25, 30, 15
	210	210, 200, 215, 190, 195	210, 200, 190, 215, 195		80	80, 85, 100, 75, 90	80, 85, 100, 75, 90
	310	310, 305, 315, 300, 295	310, 305, 315, 295, 300		45	45, 35, 40, 50, 10	45, 35, 40, 10, 50
	285	285, 280, 290, 265, 275	285, 280, 290, 275, 240		15	15, 20, 10, 5, 25	15, 20, 10, 5, 25
	145	145, 130, 135, 175, 140	145, 135, 130, 90, 140		80	80, 75, 85, 70, 45	80, 75, 85, 70, 45
	355	355, 0, 350, 15, 0	355, 350, 0, 10, 15		150	150, 155, 5, 160, 25	150, 155, 185, 25, 160
	10	10, 25, 20, 15, 5	10, 20, 15, 25, 5		130	130, 140, 270, 105, 110	130, 140, 135, 230, 125
	35	35, 20, 315, 30, 15	35, 15, 25, 30, 20		325	325, 315, 275, 330, 335	325, 315, 275, 350, 335
	340	340, 345, 290, 95, 90	345, 340, 290, 350, 285		295	295, 205, 225, 325, 245	295, 205,325, 330, 225
	305	305, 275, 295, 290, 300	305, 275, 310, 300, 295		260	250, 255, 75, 235, 265	260, 255, 75, 265, 235
	70	70, 65, 75, 90, 95	70, 75, 65, 90, 80		15	15, 20, 10, 5, 25	15, 20, 10, 5, 25

Figure A1: Top-5 active MBONs and the original orientations for all objects(Part1).







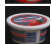
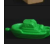
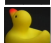

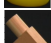



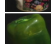



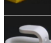
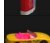




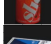
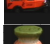

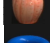
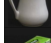


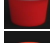

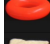
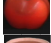
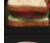
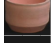
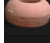
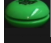
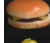
864		205°	205, 210, 215, 200, 25	205, 210, 215, 200, 195		230	230, 235, 220, 205, 225	230, 235, 220, 205, 225
865		150	150, 170, 155, 165, 100	150, 155, 175, 135, 165		205	205, 200, 210, 190, 215	205, 200, 210, 190, 215
866		210	210, 215, 220, 270, 285	210, 215, 220, 230, 225		65	65, 70, 60, 80, 55	65, 60, 55, 70, 80
867		170	170, 165, 175, 190, 180	170, 175, 165, 190, 180		10	10, 15, 20, 25, 5	10, 15, 20, 25, 5
868		45	45, 40, 50, 35, 30	45, 40, 50, 35, 30		180	180, 185, 190, 170, 140	180, 185, 190, 170, 140
869		25	25, 20, 30, 55, 10	25, 20, 30, 10, 5		175	175, 165, 120, 185, 0	175, 120, 165, 180, 220
870		135	135, 140, 145, 130, 160	135, 140, 145, 130, 160		40	40, 45, 35, 50, 25	40, 45, 50, 35, 25
871		160	160, 165, 175, 170, 155	160, 165, 175, 155, 170		5	5, 0, 10, 15, 355	5, 0, 10, 15, 20
872		130	130, 125, 310, 320, 135	130, 125, 310, 320, 315		115	115, 110, 105, 120, 125	115, 110, 120, 105, 125
873		25	25, 20, 15, 35, 30	25, 20, 15, 35, 30		170	170, 165, 160, 175, 185	170, 160, 165, 175, 185
874		45	45, 70, 60, 65, 40	45, 40, 55, 60, 65		315	315, 285, 280, 310, 290	315, 285, 320, 310, 290
875		115	115, 110, 120, 110, 130	115, 120, 110, 130, 320		175	175, 180, 170, 190, 185	175, 170, 180, 190, 185
876		195	195, 200, 190, 15, 345	195, 200, 190, 15, 345		170	170, 185, 145, 155, 180	170, 185, 145, 180, 155
877		150	150, 145, 175, 160, 155	150, 145, 185, 170, 175		220	220, 215, 180, 185, 195	220, 215, 180, 250, 185
878		120	120, 135, 130, 125, 140	120, 130, 135, 125, 155		90	95, 100, 80, 85, 60	95, 100, 85, 80, 75
879		35	35, 30, 25, 40, 45	35, 30, 25, 40, 45		315	315, 305, 285, 240, 295	315, 305, 325, 310, 320
880		185	185, 190, 180, 195, 175	185, 190, 180, 175, 195		175	175, 180, 170, 165, 185	175, 180, 170, 165, 185
881		100	100, 95, 90, 115, 110	100, 95, 90, 115, 110		85	85, 90, 100, 105, 95	85, 90, 100, 105, 70
882		40	40, 45, 25, 30, 35	40, 45, 30, 25, 35		50	50, 35, 25, 20, 45	50, 35, 45, 25, 20
883		70	70, 75, 80, 55, 35	70, 75, 55, 80, 45		180	180, 185, 190, 175, 200	180, 185, 190, 175, 195

Figure A2: Top 5 active MBONs and the original orientations for all objects(Part2).

We show all objects at an example orientation in Figure A1 and A2. The first column is the actual orientation of the object, the second column is top 5 active MBONs found by method 1, the third cloumn is method 2.

A.2.2 CROSS-VALIDATION

Model	Best accuracy on testing set	Best accuracy on training set
AlexNet	0.00	92.37
GoogleNet	0.00	87.32
VGG16	0.00	97.36
ResNet50	0.00	96.53

Table A6: Cross-validation on our modified dataset results in 0 testing accuracy.

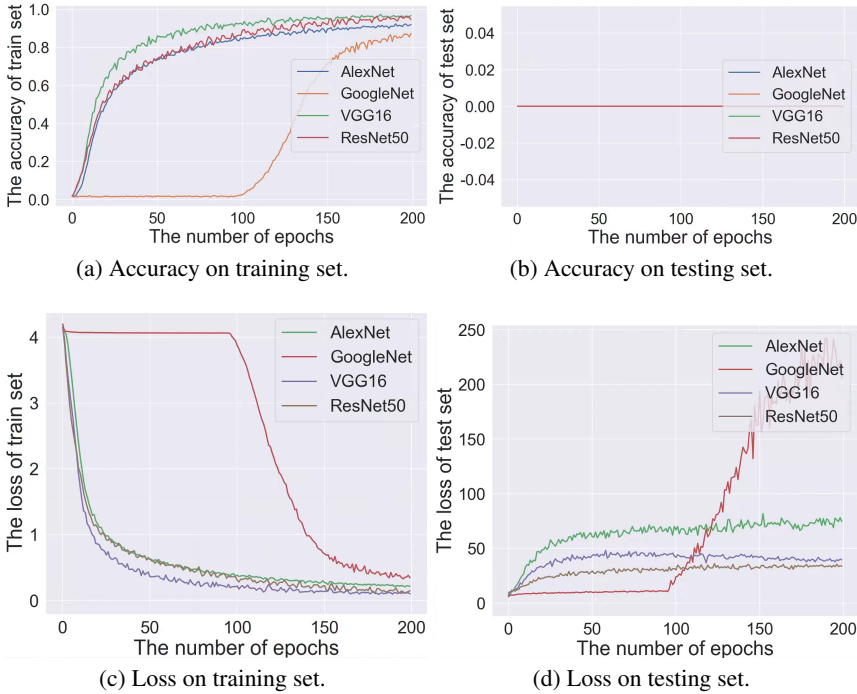
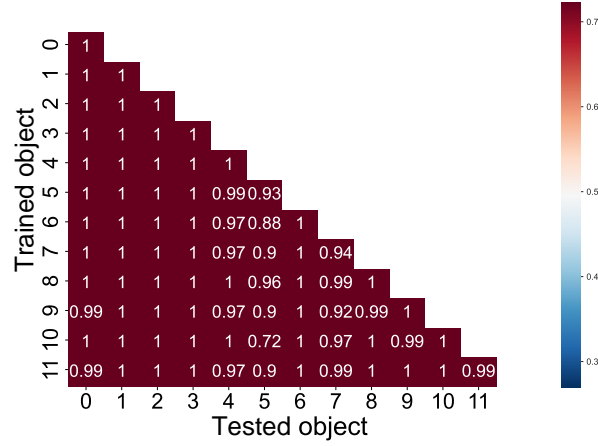
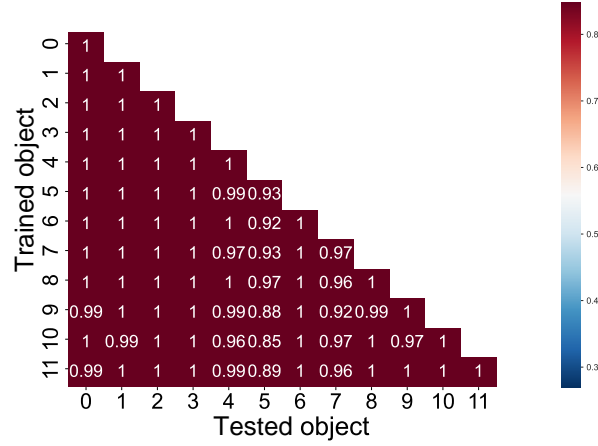


Figure A3: Cross-validation on our modified dataset results in 0 testing accuracy.



(a) Accuracy using Method 1



(b) Accuracy using Method 2

Figure A5: Accuracy of specific objects in COIL-100-AS during incremental learning. Each row represents the index of the object being trained on, and each column represents the index of the object being retrieved. (a) Accuracy using Method 1. (b) Accuracy using Method 2. Results are shown for the first 12 objects only.

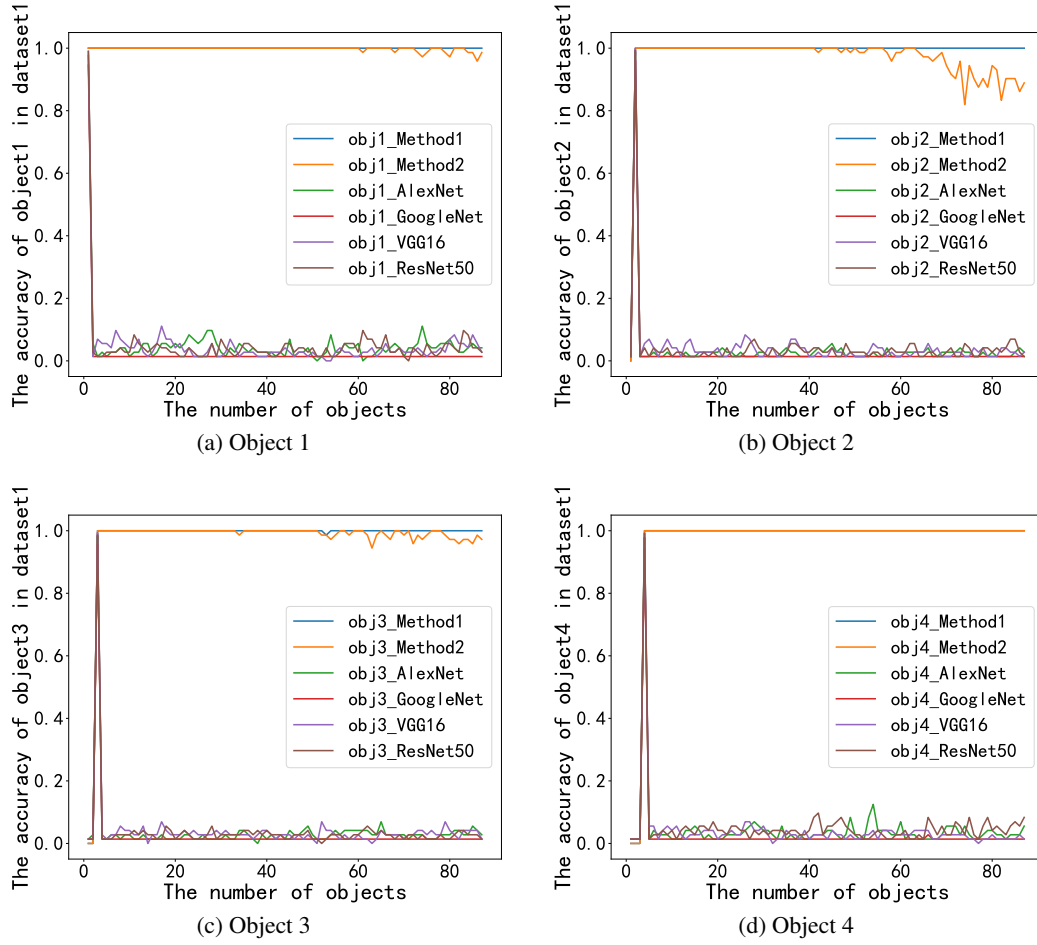


Figure A6: Accuracy of the first four objects for incremental learning.

A.2.4 ACCURACY FOR UNFAMILIAR ORIENTATIONS

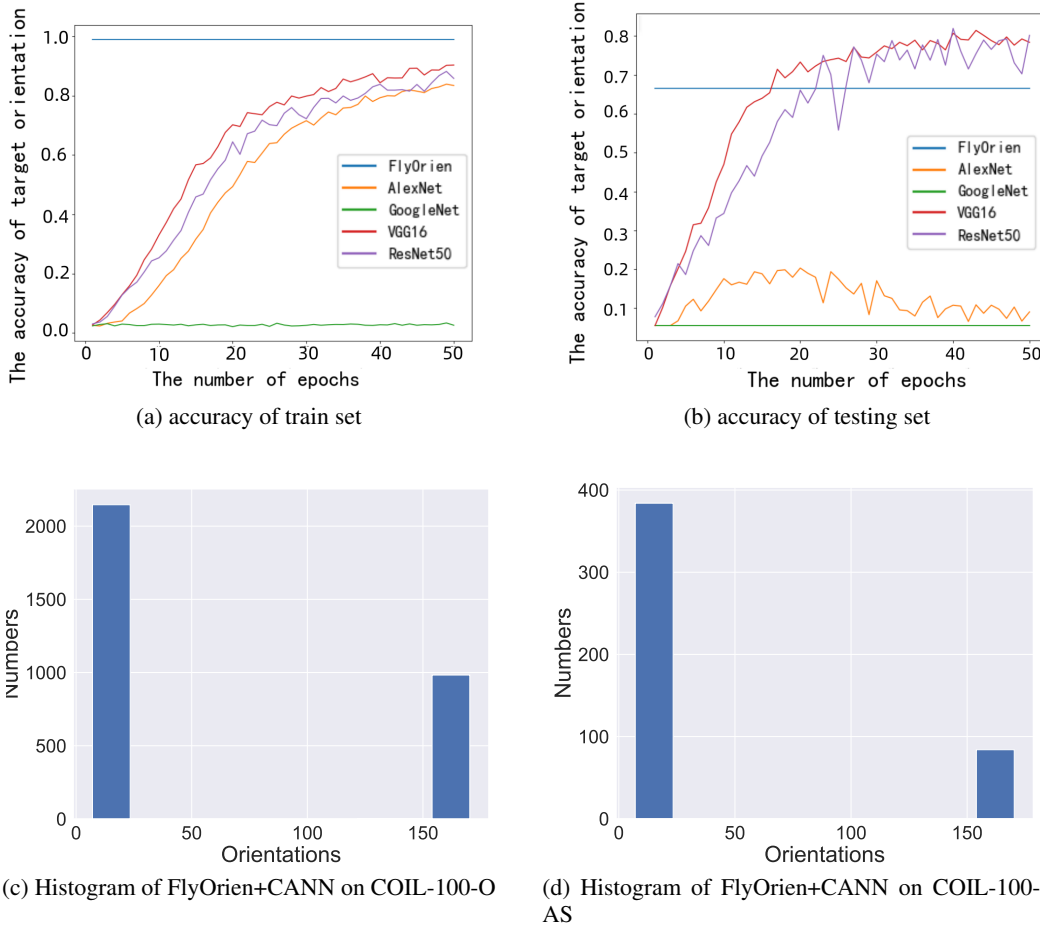


Figure A7: Accuracy of train set and testing set. FlyOri en’s accuracy can reach a high level in one-shot learning, without longtime training like other baselines

A.2.5 ACCURACY WITH CONTRAST CHANGES

Table A7: Accuracy(%) and training time(s) of our methods and four baselines when the image contrast changes on COIL-100-O.

	Method 1	Method 2	AlexNet	GoogleNet	VGG16	ResNet50
Device	CPU		GPU			
Training accuracy	92.93	91.26	90.45	85.60	96.30	96.18
Test accuracy	74.01	73.96	76.55	23.00	64.21	57.95
Difference	18.92	17.30	13.90	62.60	32.09	38.23
Training time	157.83	78.26	870.68	1850.24	10255.02	4300.81

In this task, the training set consists of original images, while the testing set contains images with modified contrast. The significant drop in test accuracy compared to training accuracy suggests overfitting. GoogleNet, VGG16, and ResNet50 exhibited more overfitting compared to our model, while AlexNet demonstrated less overfitting. Therefore, both our model and AlexNet displayed greater robustness in handling contrast changes.